

# Earth's magnetic field is probably not reversing

Maxwell Brown<sup>a,b,1</sup>, Monika Korte<sup>b</sup>, Richard Holme<sup>c,d</sup>, Ingo Wardinski<sup>b,e</sup>, and Sydney Gunnarson<sup>a</sup>

<sup>a</sup>Institute of Earth Sciences, University of Iceland, 101 Reykjavik, Iceland; <sup>b</sup>GFZ German Research Centre for Geosciences, Telegrafenberg, 14473 Potsdam, Germany; <sup>c</sup>School of Environmental Sciences, University of Liverpool, Liverpool L69 3GP, United Kingdom; <sup>d</sup>Max Planck Institute for Solar System Research, 37077 Göttingen, Germany; and <sup>e</sup>Laboratoire de Planétologie et de Géodynamique, Université de Nantes, UMR 6112 CNRS, F-44322 Nantes Cedex 3, France

Edited by Lisa Tauxe, University of California, San Diego, La Jolla, CA, and approved March 30, 2018 (received for review December 19, 2017)

The geomagnetic field has been decaying at a rate of  $\sim 5\%$  per century from at least 1840, with indirect observations suggesting a decay since 1600 or even earlier. This has led to the assertion that the geomagnetic field may be undergoing a reversal or an excursion. We have derived a model of the geomagnetic field spanning 30–50 ka, constructed to study the behavior of the two most recent excursions: the Laschamp and Mono Lake, centered at 41 and 34 ka, respectively. Here, we show that neither excursion demonstrates field evolution similar to current changes in the geomagnetic field. At earlier times, centered at 49 and 46 ka, the field is comparable to today's field, with an intensity structure similar to today's South Atlantic Anomaly (SAA); however, neither of these SAA-like fields develop into an excursion or reversal. This suggests that the current weakened field will also recover without an extreme event such as an excursion or reversal. The SAA-like field structure at 46 ka appears to be coeval with published increases in geomagnetically modulated beryllium and chlorine nuclide production, despite the global dipole field not weakening significantly in our model during this time. This agreement suggests a greater complexity in the relationship between cosmogenic nuclide production and the geomagnetic field than is commonly assumed.

geomagnetism | South Atlantic anomaly | Laschamp excursion | reversals | paleomagnetism

**R**eversals and excursions have occurred numerous times in Earth's history (1–4), and the recent behavior of the geomagnetic field has led to a discussion of whether we are in the early stages of a reversal or excursion (5–9). Since direct observations of the strength of the geomagnetic field began in 1840 (10, 11), it has decreased by  $\sim 5\%$  per century (12). This decay has been coupled to the growth and westward movement of a pronounced regional intensity low from southern Africa to South America, the so-called South Atlantic Anomaly (SAA) (see the image for the 2015 field in Fig. 1). Indirect measurements of intensity obtained from fired archeological artifacts, volcanic rocks, and sediments suggest that the current fall in intensity may have begun before 1840 (9, 13) and perhaps as early as 2,000 y ago (14). It has been suggested that the SAA may continue to grow and initiate a reversal or excursion (8). Furthermore, conditions at the core–mantle boundary (CMB) related to long-lived structures such as the large low seismic shear wave velocity province (LLSVP) below southern Africa (15) may be responsible for the occurrence of geomagnetic field structures such as the SAA (16). Given the longevity of the African LLSVP, SAA-like structures have been suggested to be a recurrent feature of the geomagnetic field and a trigger for reversals/excursions (16, 17).

Although methods to forecast the geomagnetic field are in development (18, 19), they cannot yet predict the field on long time scales. An alternative approach is to investigate the behavior of past reversals and excursions and infer whether the field structures we see today resemble those approaching reversals and excursions. As we go back in time, the amount of data describing the temporal and spatial evolution of the geomagnetic field decreases; therefore, we concentrate our analysis on the two most recent excursions, the Laschamp at  $\sim 41$  ka

(20, 21) and the Mono Lake at  $\sim 34$  ka. In this study, we present a temporally continuous global spherical harmonic model covering both the Laschamp and Mono Lake excursions and compare the geomagnetic field prior and during these excursions with today's geomagnetic field.

## Results

In Fig. 1, we show maps of (i) the current field, (ii) two snapshots of the field in a similar configuration to today (48.5 and 46.3 ka), and (iii) two periods immediately following ii that are dominated by the dipole, but do not have field structures similar to today (47.25 and 43.8 ka). These maps can be compared with snapshots of the field for the center of each excursion (Fig. 2), defined as local global minima in dipole moment (DM;  $\sim 41$  ka for the Laschamp excursion and  $\sim 34$  ka for the Mono Lake excursion) (Fig. 3). Further insights into the field structure are provided by an energy spectrum derived from the mean square field (23, 24) (*Materials and Methods*). We determined spectra at two depths: the CMB, reflecting the physical origin of the field, and the surface, reflecting what is observed (movies of the spectra are provided in [Movie S1](#)). In Fig. 4, we summarize spectra for some of the snapshots in Figs. 1 and 2.

The two excursions display complex field structures that, unlike the current field, are either not dominated by the dipole field (as during the Laschamp excursion; Fig. 4C) or have a weaker dipole contribution than today (as during the Mono Lake excursion; Fig. 4D). However, the fields at 48.5 and 46.3 ka are highly reminiscent of the historical and recent field, as seen in the global models *gufm1* (10) and the International Geomagnetic

## Significance

Earth's magnetic field is generated in Earth's convecting liquid iron outer core and protects Earth's surface from harmful solar radiation. The field has varied on different timescales throughout geological history, and these variations reflect changes deep within the Earth. Two of the field's most extreme variations are reversals and excursions. During such events, the strength of the field decreases and the magnetic poles rapidly flip polarity, with reversals characterized by the pole retaining an opposite polarity, while excursions are marked by a return to the original polarity. Field strength over the past centuries has also been decreasing strongly; however, through analyzing previous excursions, we infer that Earth's magnetic field is not in an early stage of a reversal or excursion.

Author contributions: M.B. designed research; M.B., M.K., and S.G. performed research; M.B., M.K., R.H., I.W., and S.G. analyzed data; and M.B., M.K., R.H., I.W., and S.G. wrote the paper.

The authors declare no conflict of interest.

This article is a PNAS Direct Submission.

Published under the PNAS license.

Data deposition: The data (a .zip file containing .txt files) have been deposited at the German Research Center for Geosciences Data Service ([doi.org/10.5880/GFZ.2.3.2018.002](https://doi.org/10.5880/GFZ.2.3.2018.002)).

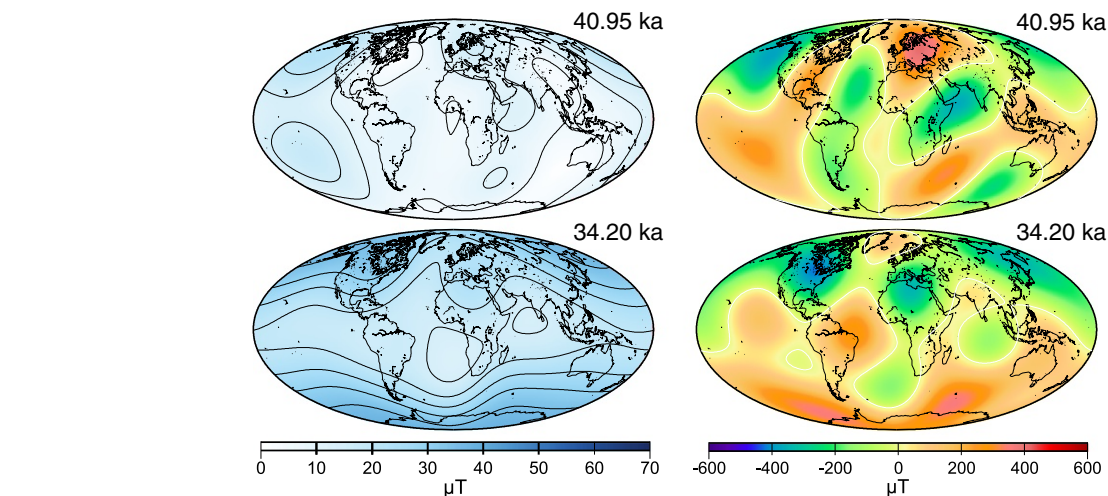
<sup>1</sup>To whom correspondence should be addressed. Email: [maxwell@hi.is](mailto:maxwell@hi.is).

This article contains supporting information online at [www.pnas.org/lookup/suppl/doi:10.1073/pnas.1722110115/-DCSupplemental](https://www.pnas.org/lookup/suppl/doi:10.1073/pnas.1722110115/-DCSupplemental).

Published online April 30, 2018.







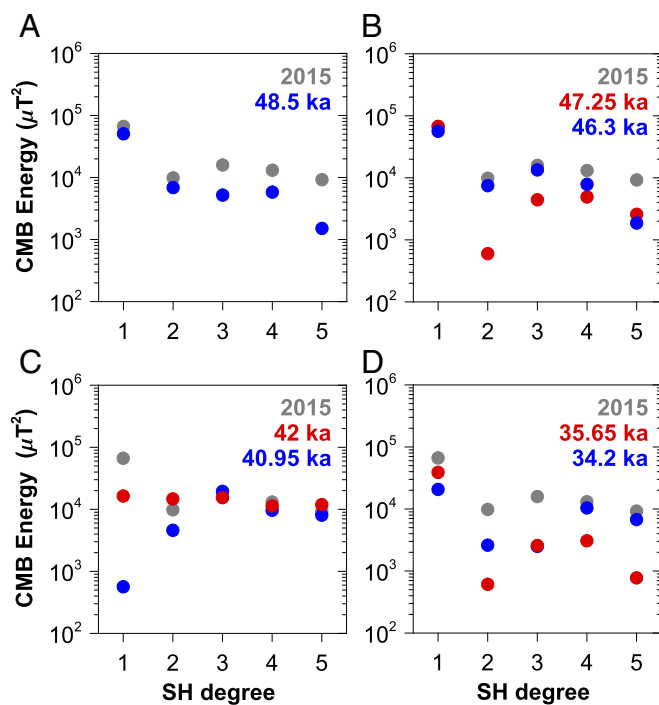


**Fig. 4.** (A–D) Mean square field energy spectrum variations through spherical harmonic (SH) degrees 1–5 (*Materials and Methods*). SH degree 1 is the dipole term. (B–D) Red symbols are times preceding the 46-ka SAA epoch (B), the Laschamp excursion (C), and the Mono Lake excursion (D). Blue symbols are for times during the 49- and 46-ka SAA epochs and at the midpoints of the two excursions. Gray symbols are for the 2015 IGRF-12 (22) field as a reference for today's field spectrum.

in the octupole term matches the energy of the dipole term. However, the Mono Lake excursion is not driven into a more substantial excursion, and by 33 ka, the field regains its dominantly dipolar appearance at the surface, although increased energy in some of the higher-order components post-33 ka creates greater spatial complexity in both intensity and *Br* than for today's field.

**A Mechanism for Excursion and Reversal Generation.** A possible interpretation for excursions is that field contributions of all scales vary with time, but with a weaker base state (a weaker axial dipole), variations in the axial dipole are sufficient to produce an excursion (27). Excursions can therefore be considered a part of normal secular variation, but with a weaker axial dipole contribution and a greater chance of producing a zero or reversed dipole field. We argue that the field has two possible mean states, one in which the axial dipole is dominant at the CMB, which is broadly stable, and one in which the axial dipole matches the higher degrees, when fluctuations in the axial dipole can produce an excursion. The question remains: Are random fluctuations sufficient for a full reversal? To answer this question, a reexamination of the most recent reversal, the Matuyama–Brunhes, building on previous modeling (30), but with an expanded dataset, will be necessary.

We infer that for excursions to occur, a weakening of the field across much of the globe spreading from multiple sources is required, and not just localized weakening expanding from an SAA-like feature. They also require the growth of reversed flux patches in both hemispheres, with reversed flux transiting the poles. However, the amount and duration of reversed flux across the poles differs for the Laschamp and Mono Lake excursions. Reversed flux occurs simultaneously across both poles during the Laschamp (Fig. 2) and is present for ~2 ka,

whereas across the Mono Lake, reversed flux is located primarily over the North Pole (Fig. 2) for only a few hundred years (*Movie S1*).

Although today's dipole is weakening, it is still substantially stronger than the higher-degree components of the field and exceeds the dipole moment from our model through the majority of 40–50 ka. Today's secular variation is instead comparable to the SAA-like states at 49 and 46 ka, which did not lead to an excursion. Similar arguments apply to the Mono Lake excursion; although it does not reach the magnitude and extent of the Laschamp excursion, it still starts from a more geographically spread weak state than from a single SAA-like feature.

**Relationship Between SAA-Like Structures and Cosmogenic Nuclide Production.** The above inferences depend on the robustness of our model; however, there is evidence from a complementary source: variations in cosmogenic nuclide production. Peaks in nuclide production ( $^{10}\text{Be}$  and  $^{36}\text{Cl}$ ) coincide with the intensity lows of the Laschamp (29, 31) and Mono Lake (31, 32) excursions (Fig. 3C). However, there are also peaks in production that do not match known excursions. One production peak of particular note occurs at 46 ka and is coeval with one of our SAA-like structures, supporting our observation of a weakened field at this time. This peak is evident as a low in the 1/800 y filtered  $^{10}\text{Be}$ - and  $^{36}\text{Cl}$ -derived dipole variations obtained from Greenland ice core records (7, 28) and is hinted at in the stacks of sediment  $^{10}\text{Be}/^9\text{Be}$  records from the Portuguese margin and west equatorial Pacific (29) (Fig. 3C). There are two other times when there are decreases in both the  $^{10}\text{Be}$ - and  $^{36}\text{Cl}$ -derived dipole data. The low at ~31 ka is approximately coeval with a decrease in DM in our model. The low at ~37 ka does not appear to be correlated with any field behavior in our model; however, this low appears negligible in the same records filtered at 1/3,000 y (31). The origin of the anticorrelation of the  $^{10}\text{Be}$ - and  $^{36}\text{Cl}$ -derived dipole ice core records between 49 and 50 ka is currently unknown (31), and we do not consider cosmogenic nuclide data before 48 ka in our analysis.

Cosmogenic nuclide records reflect globally averaged production through postproduction atmospheric mixing processes (33). Numerous factors can influence cosmogenic nuclide production and concentration (31). On time scales longer than hundreds of years, production results primarily from variations in the geomagnetic field, although possible millennial-scale solar activity and climate influences may complicate estimates of dipole change (31). It is commonly assumed that production is related to changes in the dipole component of the field. This is based on the altitude of modulation of cosmic rays and the rapid fall-off of non-dipole components with distance from the CMB (31). However, we observe only a minor reduction in DM at 46 ka in our model (Fig. 3) and suggest instead that localized areas of weak intensity, such as SAA-like structures, might additionally allow cosmogenic nuclides to penetrate the geomagnetic field. We do not claim that the apparently coeval timing of one our SAA-like structures with a period of increased cosmogenic nuclide production unequivocally links the two events; however, this observation would be worth pursuing by researchers in the future. This conjecture could be tested by incorporating the geomagnetic model presented here into models of cosmogenic nuclide production for this time.

## Materials and Methods

The data used for modeling can be found at [doi.org/10.5880/GFZ.2.3.2018.002](https://doi.org/10.5880/GFZ.2.3.2018.002). Our analysis derives from a model of the time-dependent geomagnetic field spanning 30–50 ka. The model was constructed from the largest compilation of sediment and volcanic paleomagnetic data for this period to date (*SI Appendix*), exceeding the amount of data used in the only previous attempt to model the Laschamp excursion (34). An inverse model was constructed by using a spherical harmonic decomposition of the scalar potential

for the field  $B = \nabla \Phi$ , with each coefficient expanded in time on a basis of cubic B-splines, following methods used for the historical (10) and Holocene field (14, 35, 36). The spatial series was expanded to spherical harmonic degree and order 10, and spline knot points were placed every 50 y. This allowed for more complexity in the model than we expected to recover from the available data. Regularizations in space and time were invoked to trade off a reasonable fit to the data against smooth models, i.e., those requiring the least amount of structure to describe the data. We used physically motivated regularization constraints: the Ohmic dissipation norm in space and the second derivative of the radial field component in time. The model coefficients were determined from the data under the regularization constraints by using a least-squares approach. Declination, inclination, and intensity data were nonlinearly related to the model coefficients; therefore, the problem was linearized and the solution found iteratively. The model was based on 35 iteration steps to ensure convergence (37). This description allows us to plot maps both of the field observed at Earth's surface and the radial magnetic field ( $Br$ ) at the CMB, the region of the field's origin. (Movies of  $Br$  at the CMB and total field strength at Earth's surface are provided in [Movie S1](#).)

The data uncertainties are insufficiently defined to be used to constrain the appropriate smoothness of the model through a given fit to the data. Instead, following previous Holocene geomagnetic field modeling (37), the spatial damping parameter was chosen by comparing the main-field energy spectra at times before and after the Laschamp excursion with the present-day spectrum. This ensured that for degree  $\geq 2$ , the energy in each degree was not substantially higher than for the present-day field (37). With our chosen regularization constraint, the spectrum falls off rapidly beyond spherical harmonic degrees 4 or 5, suggesting that the data are insufficient for effective model resolution beyond these degrees. All model output in the figures have been truncated to degree 5. To test whether our model is capable of resolving SAA-like field structures up to degree 5, we truncated the IGRF-12 model for 2015 to different spherical harmonic degrees. The surface intensity anomaly is visible even at degree 2, with radial field structures appearing at degrees 4 and 5 (see [SI Appendix](#) for further details on this test).

Given the inherent temporal smoothing of the paleomagnetic signal in sediment data (depending on sedimentation rate and other mechanisms affecting remanence acquisition and/or sampling/measurement method), the secular variation energy will be lower than for models of the present-day geomagnetic field. We chose the strength of temporal regularization through a visual comparison of data and model predictions, such that the model on average did not show more temporal variability than reasonably required by the data ([SI Appendix](#), Figs. S4–S6 and S10–S12).

The parameters used to describe magnetic field evolution are as follows. The mean square field (23, 24) is given by

$$\int B(r)^2 d\Omega = \sum_l^{l_{\max}} (l+1) \left(\frac{a}{r}\right)^{2l+4} \sum_{m=0}^l [(g_l^m)^2 + (h_l^m)^2], \quad [1]$$

where  $g_l^m$  and  $h_l^m$  are the Schmidt-normalized Gauss coefficients of spherical harmonic degree  $l$  and order  $m$ ,  $a$  is the radius to be investigated, and  $r$  is the mean radius of the solid Earth. In Fig. 4 the contributions to this quantity are separated by spherical harmonic degree, and the energy at each degree,  $l$ , is plotted against that degree. The energy of the dipole ( $R_d$ ) and non-dipole ( $R_{nd}$ ) field plotted in Fig. 3 are limited to degree and order 5 and are given by

$$R_d = 2 \left(\frac{a}{r}\right)^6 (g_1^0)^2 + (g_1^1)^2 + (h_1^1)^2 \quad [2]$$

and

$$R_{nd} = \sum_{l=2}^5 \left[ (l+1) \left(\frac{a}{r}\right)^{2l+4} \sum_{m=0}^l ((g_l^m)^2 + (h_l^m)^2) \right]. \quad [3]$$

The DM at Earth's surface plotted in Fig. 3 is given by

$$DM = \frac{4\pi}{\mu_0} a^3 \sqrt{(g_1^0)^2 + (g_1^1)^2 + (h_1^1)^2}, \quad [4]$$

where  $\mu = 4\pi \cdot 10^{-7}$  Vs/Am, the permeability of free space. The latitude of the dipole axis (DT) plotted in Fig. 3 is given by

$$DT = \tan^{-1} \left( \frac{g_1^0}{\sqrt{(g_1^1)^2 + (h_1^1)^2}} \right). \quad [5]$$

**ACKNOWLEDGMENTS.** We thank Sanja Panovska and Lisa Tauxe for providing their data compilations and the authors of individual studies who provided data. M.B. acknowledges discussions with Norbert Nowaczyk and Roman Leonhardt. This work was supported by Deutsche Forschungsgemeinschaft SPP PlanetMag 1488 Project BR4697/1. R.H. was supported by a Gauss Professorship from the Akademie der Wissenschaften zu Göttingen. I.W. was supported by Agence Nationale de la Recherche Project ANR-13-BS05-0012 (Marmite).

- Cande SC, Kent DV (1995) Revised calibration of the geomagnetic timescale for the late Cretaceous and Cenozoic. *J Geophys Res* 100:6093–6095.
- Laj C, Channell JET (2007) Geomagnetic excursions. *Treatise on Geophysics*, ed Schubert G (Elsevier, Amsterdam), pp 373–416.
- Ogg J (2012) Geomagnetic polarity time scale. *The Geologic Time Scale*, eds Gradstein FM, Ogg JG, Schmitz MD, Ogg GM (Elsevier, Boston), pp 85–113.
- Singer BS (2014) A Quaternary geomagnetic instability time scale. *Quat Geochronol* 21:29–52.
- Hulot G, Eymin C, Langlais B, Manda M, Olson N (2002) Small-scale structure of the geodynamo inferred from Oersted and Magsat satellite data. *Nature* 416:620–623.
- Constable C, Korte M (2006) Is Earth's magnetic field reversing? *Earth Planet Sci Lett* 246:1–16.
- Laj C, Kissel C (2015) An impending geomagnetic transition? Hints from the past. *Front Earth Sci* 3:61.
- Pavón-Carrasco FJ, De Santis A (2016) The South Atlantic Anomaly: The key for a possible geomagnetic reversal. *Front Earth Sci* 4:40.
- Poletti W, Biggin AJ, Trindade RI, Hartmann GA, Terra-Nova F (2018) Continuous millennial decrease of the earth's magnetic axial dipole. *Phys Earth Planet Inter* 274:72–86.
- Jackson A, Jonkers ART, Walker MR (2000) Four centuries of geomagnetic secular variation from historical records. *Philos Trans R Soc Lond A* 358:957–990.
- Jonkers ART, Jackson A, Murray A (2003) Four centuries of geomagnetic data from historical records. *Rev Geophys* 41:1006.
- Gubbins D, Jones A, Finlay CC (2006) Fall in the Earth's field is erratic. *Science* 312:900–902.
- Suttie N, Holme R, Hill MJ, Shaw J (2011) Consistent treatment of errors in archaeointensity implies rapid decay of the dipole prior to 1840. *Earth Planet Sci Lett* 304:13–21.
- Constable C, Korte M, Panovska S (2016) Persistent high paleosecular variation activity in southern hemisphere for at least 10 000 years. *Earth Planet Sci Lett* 453:78–86.
- Garnero EJ, McNamara AK (2008) Structure and dynamics of Earth's lower mantle. *Science* 320:626–628.
- Tarduno JA, et al. (2015) Antiquity of the South Atlantic Anomaly and evidence for top-down control on the geodynamo. *Nat Commun* 6:7865.
- Gubbins D (1987) Mechanism for geomagnetic polarity reversals. *Nature* 326:167–169.
- Fournier A, et al. (2010) An introduction to data assimilation and predictability in geomagnetism. *Space Sci Rev* 155:247–291.
- Tangborn A, Kuang W (2018) Impact of archeomagnetic field model data on modern era geomagnetic forecasts. *Phys Earth Planet Inter* 276:2–9.
- Singer BS, et al. (2009)  $^{40}\text{Ar}/^{39}\text{Ar}$ , K-Ar and  $^{238}\text{Th}$ - $^{232}\text{Th}$  U dating of the Laschamp excursion: A radioisotopic tie-point for ice core and climate chronologies. *Earth Planet Sci Lett* 286:80–88.
- Lascu I, Feinberg JM, Dorale JA, Cheng H, Edwards RL (2016) Age of the Laschamp excursion determined by U-Th dating of a speleothem geomagnetic record from North America. *Geology* 44:139–142.
- Thébault E, et al. (2015) International geomagnetic reference field: The 12th generation. *Earth, Planets Space* 67:79.
- Lowes FJ (1966) Mean-square values on sphere of spherical harmonic vector fields. *J Geophys Res* 71:2179–2179.
- Lowes FJ (1974) Spatial power spectrum of the main geomagnetic field, and extrapolation to the core. *Geophys J R Astr Soc* 36:717–730.
- Olson P, Amit H (2006) Changes in earth's dipole. *Naturwissenschaften* 93:519–542.
- Heitzler JR, Allen JH, Wilkinson DC (2002) Ever-present South Atlantic Anomaly damages spacecraft. *Eos, Trans Am Geophys Union* 83:165–169.
- Brown MC, Korte M (2016) A simple model for geomagnetic field excursions and inferences for palaeomagnetic observations. *Phys Earth Planet Inter* 254:1–11.
- Laj C, Guillou H, Kissel C (2014) Dynamics of the earth magnetic field in the 10–75 kyr period comprising the Laschamp and Mono Lake excursions: New results from the French Chaîne des Puys in a global perspective. *Earth Planet Sci Lett* 387:184–197.
- Ménabréaz L, Bourlès DL, Thouveny N (2012) Amplitude and timing of the Laschamp geomagnetic dipole low from the global atmospheric  $^{10}\text{Be}$  overproduction: Contribution of authigenic  $^{10}\text{Be}/^9\text{Be}$  ratios in west equatorial Pacific sediments. *J Geophys Res* 117:B111101.
- Leonhardt R, Fabian K (2007) Paleomagnetic reconstruction of the global geomagnetic field evolution during the Matuyama/Brunhes transition: Iterative Bayesian inversion and independent verification. *Earth Planet Sci Lett* 253:172–195.

